Supporting Information for:

Single-Molecule Super-Resolution Microscopy Reveals How Light Couples to a Plasmonic Nanoantenna on the Nanometer Scale

*Esther Wertz, Benjamin P. Isaacoff, Jessica D. Flynn, and Julie S. Biteen**

Department of Chemistry, University of Michigan, Ann Arbor, Michigan 48109-1055

*Email: jsbiteen@umich.edu

Contents

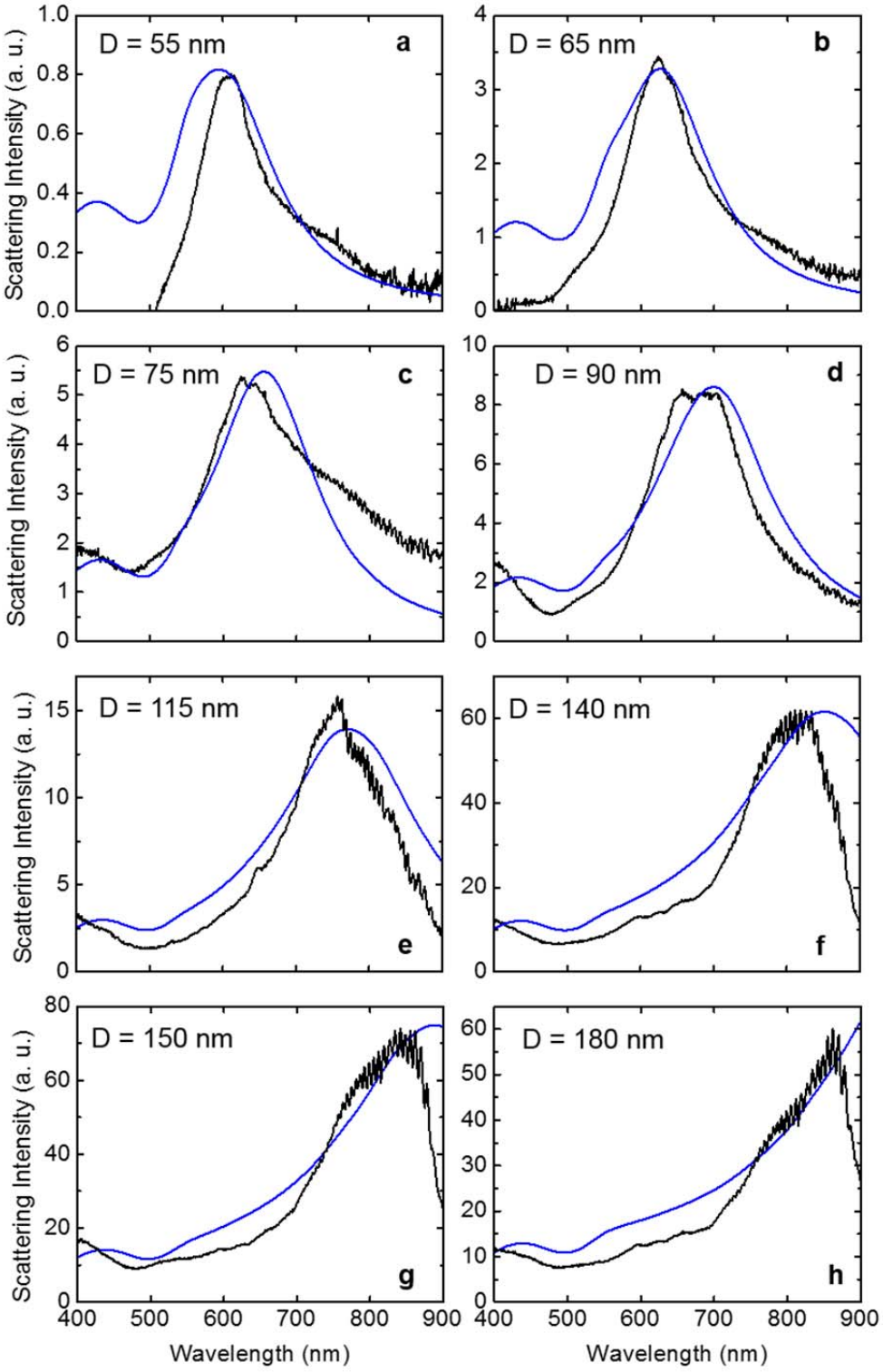

Figure S1. Localized surface plasmon resonances of gold nanoislands. Measured darkfield spectra of (a) 55-nm, (b) 65-nm, (c) 75-nm, (d) 90-nm, (e) 115-nm, (f) 140-nm, (g) 150-nm, and (h) 180-nm diameter NIs (black lines) and the corresponding calculated scattering cross-sections from finite-difference time-domain simulations (blue lines).

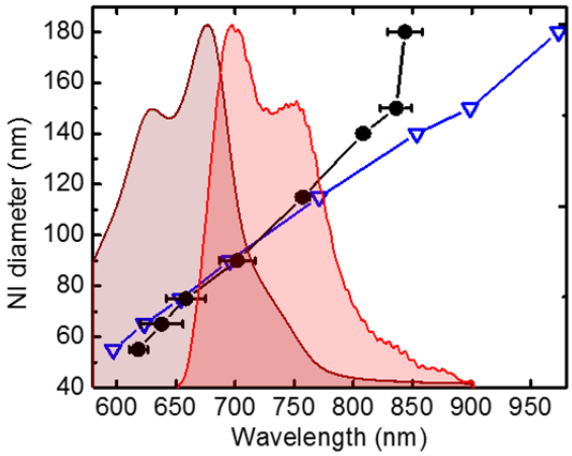

Figure S2. Dye-localized surface plasmon resonance (LSPR) detuning. Measured peak LSPR wavelengths (filled black circles) and corresponding calculated peak LSPR wavelengths (open blue triangles) for the different nanoisland diameters in Figure S1. The experimental error bars represent the standard deviation of the peak LSPR wavelength over five separate darkfield scattering measurements. The measured bulk Cy5.5 dye absorption (dark red) and fluorescence emission (light red) spectra are plotted on the same graph.

The experimental and simulated results diverge for the 140-nm, 150-nm and 180-nm NIs due to the poor quantum efficiency of the EMCCD camera above 850 nm; the more subtle differences at shorter wavelengths are most likely due to decreased signal-to-noise in the small-island scattering experiments.

In the vicinity of the NIs, plasmon-enhanced emission is expected to be maximal when the dye-LSPR detuning is close to zero, i.e., for dye molecules proximal to NIs whose peak LSPR wavelengths are located in the light red area. Plasmon-enhanced absorption is possible for dye molecules in the vicinity of the NIs with peak LSPR values in the dark red area. In our experiments, maximum enhancement is observed for the 90-nm diameter NIs, for which both the absorption and emission of Cy5.5 are expected to be enhanced. For large dye-LSPR detunings, i.e., for NIs with peak resonances above 800 nm in the present case, no enhancement is expected.

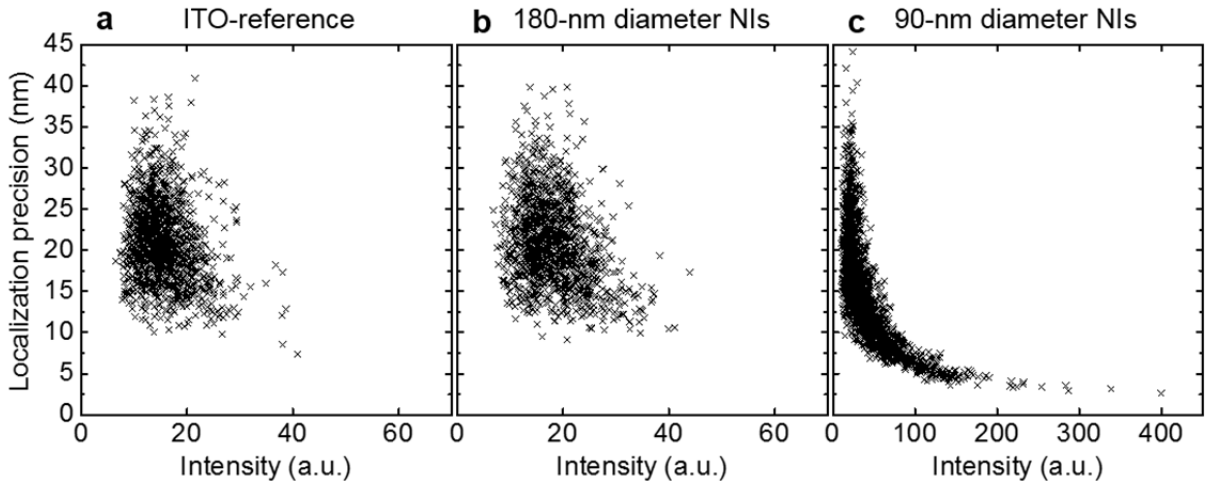

Figure S3. Single-molecule localization precision as a function of fluorescence intensity. (a) Cy5.5 on ITO-reference, (b) Cy5.5 near 180-nm diameter nanoislands, and (c) Cy5.5 near 90-nm diameter NIs. The localization precision plotted here and referenced throughout the text is the statistical 95 % confidence interval of the center of each single-molecule fit (Methods). The measured localization precision scales with the inverse of the square root of the emission intensity, consistent with theory (Thompson, Larson and Webb, *Biophys. J.*, **2002**).

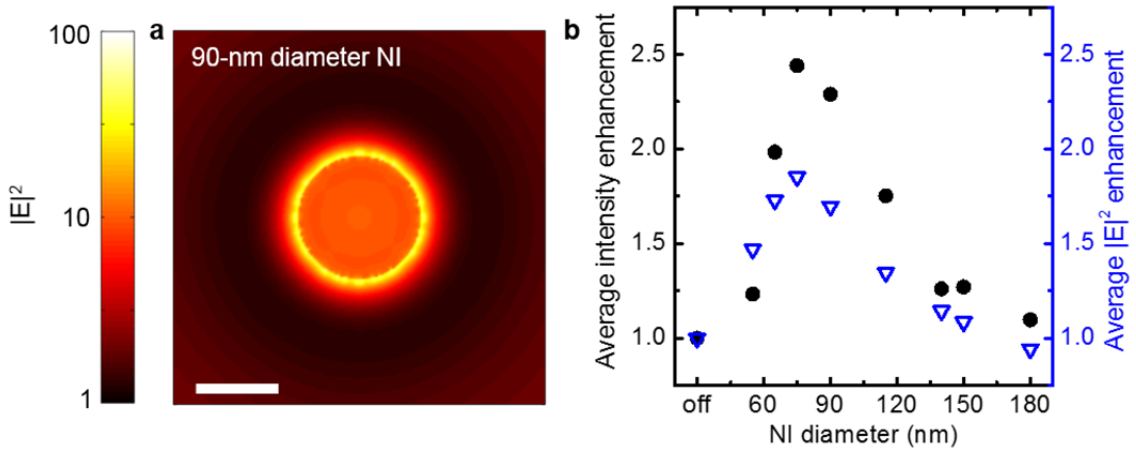

Figure S4. Finite difference time-domain (FDTD) calculations of the enhanced field about gold nanoislands at the laser excitation wavelength. (a) FDTD calculation of local field intensity at 640 nm around a 90-nm diameter gold NI excited by a plane wave. Scale bar: 50 nm. (b) Calculated average field intensity enhancement (open triangles) and measured average fluorescence intensity enhancement (filled circles) for different NI diameters. The field intensity enhancement is obtained by simulating the field intensity in the presence and absence of the Ti/Au NI, and taking the ratio of these fields at each point in space. The average field enhancement is then calculated by taking the average of the field over the area surrounding the NI.

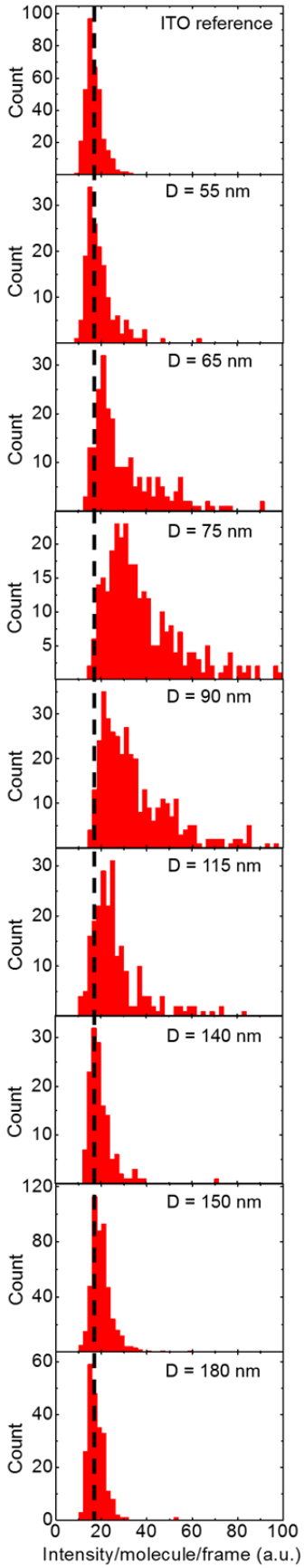

Figure S5. Distribution of measured single Cy5.5 fluorescence rates (fluorescence intensity/40 ms) upon coupling to gold nanoislands of increasing diameter, *D*, as noted. The top panel corresponds to the fluorescence rate distribution of Cy5.5 adsorbed on an ITO-coated coverslip reference, and the dashed black line is a guide to the eye for the average reference rate.

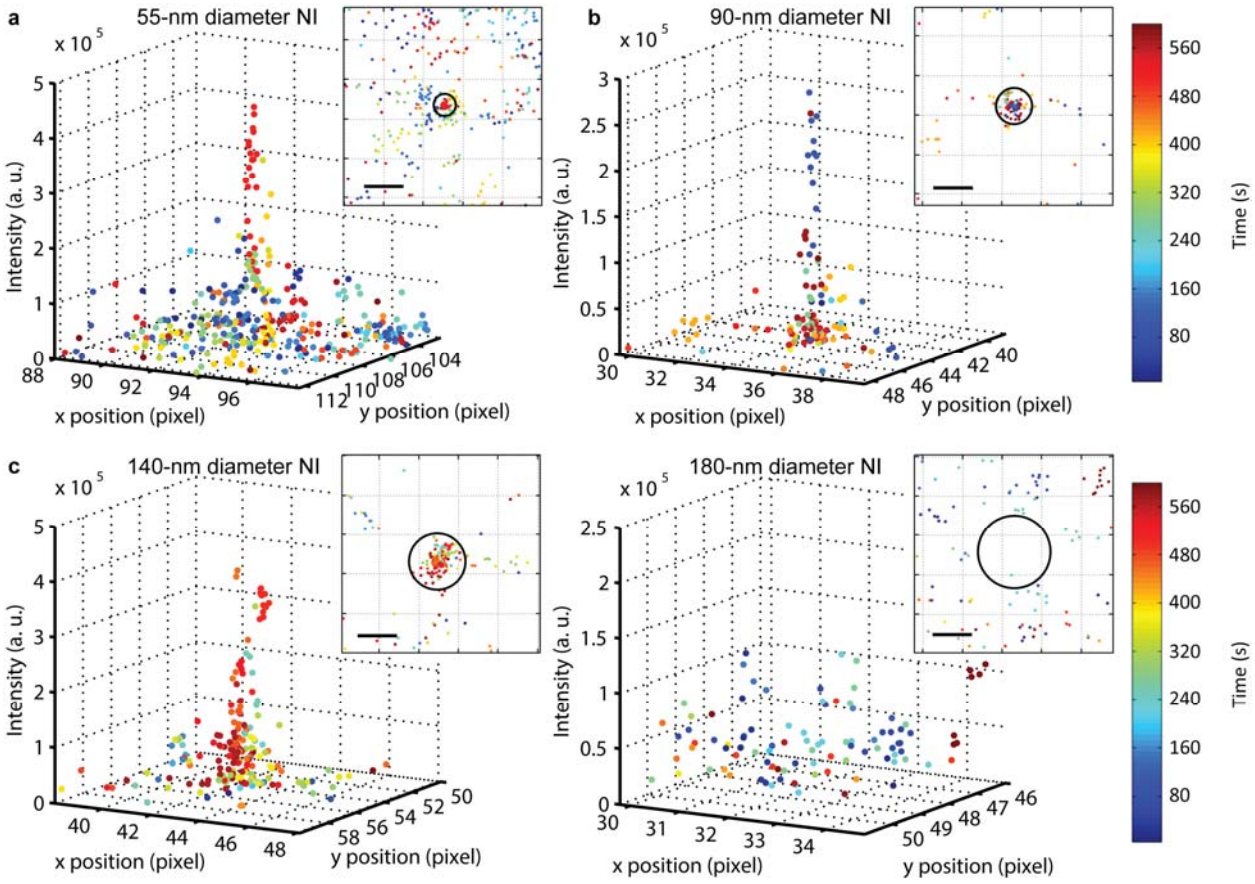

Figure S6. PAINT super-resolution maps of dye adsorbed near single nanoislands. Each dot shows the position of a single Cy5.5 dye molecule adsorbing on the sample surface. The *x* and *y* positions correspond to apparent emission position, and the *z* axis gives the integrated intensity of the molecule emission. 1 pixel = 49 nm. (a) 55-nm diameter NI; (b) 90-nm diameter NI; (c) 140-nm diameter NI; (d) 180-nm diameter NI; the insets show the corresponding top views, the black circles indicate the NI sizes. Scale bars: 2 pixels = 98 nm. The colorbar timestamp shows that sample drift during the experiment is negligible (one imaging frame = 40 ms).

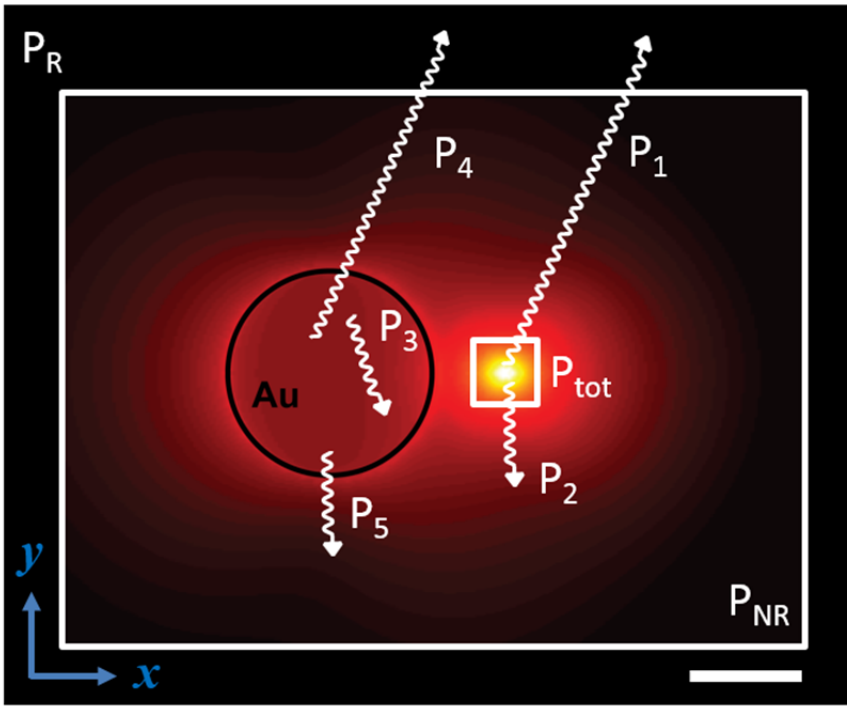

Figure S7. Power dissipation pathways in the dipole simulations. FDTD calculation of local field intensity around a 90-nm diameter gold nanoisland excited by a dipole emitter oriented in the *x* direction (perpendicular to the NI edge) at r_e = 30 nm from the NI edge, on resonance at λ = 700 nm. Scale bar: 50 nm. The white arrows represent the available decay pathways relevant to the simulations. The total power radiated into the far-field ($P_R = P_1 + P_4$) and the total power in the simulation ($P_{tot} = P_R + P_{NR} = P_1 + P_2 + P_3 + P_4 + P_5$) are measured in the presence of the NI, and the corresponding reference quantities ($P_R^0 = P_1^0$ and $P_{tot}^0 = P_R^0 + P_{NR}^0 = P_1^0 + P_2^0$) are measured for a dipole on an ITO substrate. The different power dissipation pathways are:

P_1: the power radiated into the far-field directly from the dipole,

P_2: the power lost due to nonradiative energy transfer to the environment from the dipole,

P_3: the power coupled to the NI and then dissipated due to Au material losses,

P_4: the power coupled to the NI and then radiated into the far-field, and

P_5: the power coupled to the NI and then lost due to nonradiative energy transfer to the environment.

The radiated power enhancement, *R*, and the efficiency modification, *H,* are defined as:

$$R = \frac{P_R}{P_R^0} = \frac{P_1 + P_4}{P_1^0} \qquad H = \frac{\eta_a}{\eta_a^0} = \frac{P_R}{P_{tot}}\frac{P_{tot}^0}{P_R^0} = \frac{P_1 + P_4}{P_1 + P_2 + P_3 + P_4 + P_5}\frac{P_1^0 + P_2^0}{P_1^0}$$

The power coupled to the NI then radiated to the far field, P_4, normalized by the reference radiated power, P_1^0, is defined as $A_P = P_4/P_1^0$, and as detailed below, in the limit where the dipole is very close or very far from the NI edge, the plasmon amplitude can be simplified to:

$$A_p \approx R - H.$$

Case 1: Small Dipole Separation Limit

In the limit where the dipole is very close to the NI, there is a lot of coupling. Here, $P_{tot} \gg P_R$ because the Au material losses, P_3, scale with the amount of coupling. Additionally, since P_{tot}^0 and P_R^0 differ only by the small losses to the ITO (P_2^0), $P_{tot}^0 \approx P_R^0$, and thus $\frac{P_{tot}}{P_R} \gg \frac{P_{tot}^0}{P_R^0}$. Using this inequality and recalling the definition of *H* above:

$$H = \frac{P_R}{P_{tot}} \frac{P_{tot}^0}{P_R^0} \ll 1$$

In this limit, most of the light emitted from the dipole is reradiated through the NI ($P_4 \gg P_1$). Moreover, $P_4 \gg P_1^0$, due to plasmon-enhanced emission. Then,

$$R = \frac{P_1 + P_4}{P_1^0} \approx \frac{P_4}{P_1^0} \gg 1$$

Combining these two equations, we find that:

$$R - H \approx \frac{P_4}{P_1^0} = A_P$$

Case 2: Large Dipole Separation Limit

In the limit where the dipole is very far from the NI, there is very little coupling between the dye and the plasmon. This implies that $P_3, P_4, P_5 \approx 0$ and therefore $P_1, P_2 \gg P_3, P_4, P_5$.

As a result:

$$R \approx \frac{P_1}{P_1^0} \qquad H \approx \frac{P_1}{P_1 + P_2} \frac{P_1^0 + P_2^0}{P_1^0}$$

Furthermore, in this limit, the dipole approaches its reference case behavior where $P_1 \approx P_1^0$ and $P_2 \approx P_2^0$, and so $R \approx H \approx 1$ and consequently $R - H \approx 0$. Which is consistent with the behavior of A_p where

$$A_p = \frac{P_4}{P_1^0} \approx \frac{P_4}{P_1} \approx 0$$

and thus $R - H \approx A_P$.

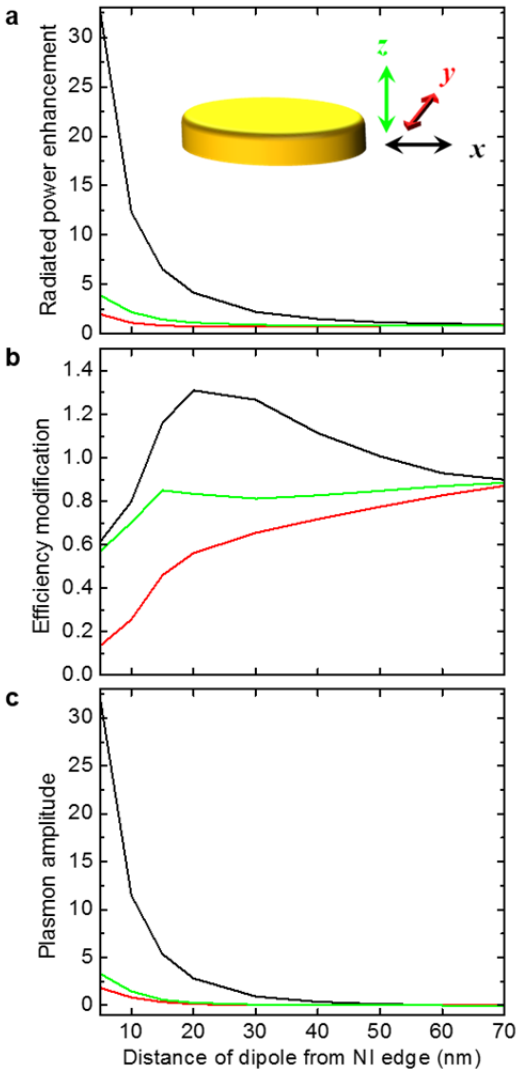

Figure S8. FDTD calculation results for each of the three orthogonal dipole orientations as a function of the distance of the dipole from the edge of a 90-nm nanoisland, on resonance at λ = 700 nm. The inset illustrates the direction of the three dipole orientations with respect to the NI; the dipole oriented in the *x* direction is plotted in black, the dipole oriented in the *y* direction is plotted in red, and the dipole oriented in the *z* direction is plotted in green. (a) Radiated power enhancement, *R*; (b) efficiency modification, *H*; (c) plasmon amplitude, A_p.

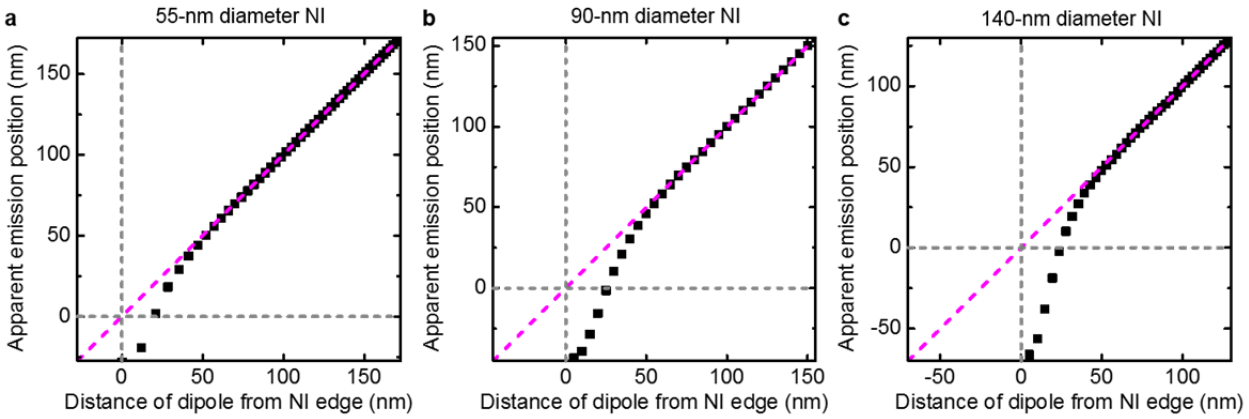

Figure S9. Apparent emission position as a function of the distance of the dipole from the nanoisland edge. (a) For D = 55 nm NIs; (b) for D = 90 nm NIs; (c) for D = 140 nm NIs. The grey dashed lines indicate the NI edge and the violet dashed line shows the $y = x$ (no mislocalization) curve.

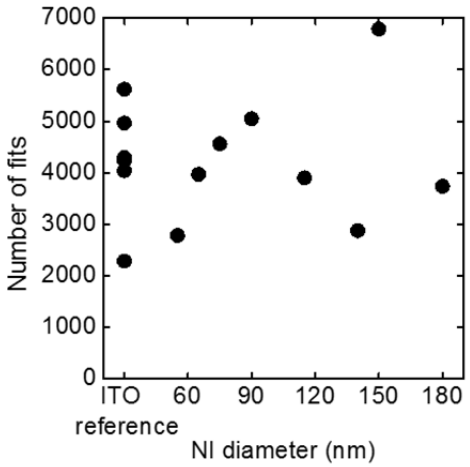

Figure S10. Number of molecules detected during single-molecule detection movies. Each square gives the number of Cy5.5 dye molecules detected over a 15 μm^2 area during a single 2-minute movie. Concentration of Cy5.5 dye in the solution: 15 nM.

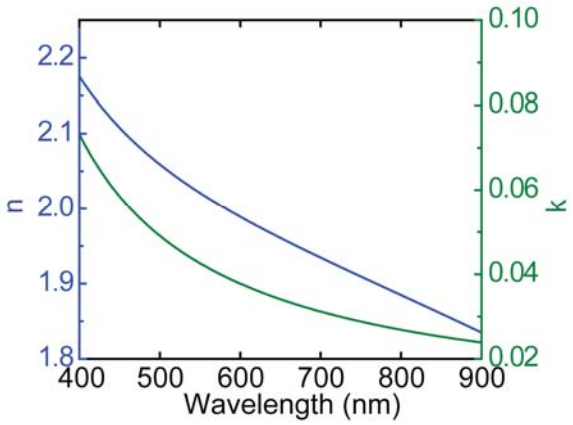

Figure S11. Spectroscopic ellipsometry characterization of a 100-nm thick indium tin oxide (ITO) film on a glass coverslip. Blue line: real part of the refractive index, *n*; green line: imaginary part of the refractive index, *k*.

Movie 1. FDTD calculations of the radiated power enhancement as a function of nanoisland diameter and wavelength, for different dipole to NI edge distances, r_e.

Movie 2. FDTD calculations of the radiated power enhancement as a function of dipole to nanoisland edge distance and wavelength, for different NI diameters, D.